Phys Chem Minerals (2006) 33: 178–191
DOI 10.1007/s00269-006-0066-1

ORIGINAL PAPER

Mariko Nagashima · Takahiro Ishida
Masahide Akasaka

Distribution of Fe among octahedral sites and its effect on the crystal structure of pumpellyite

Received: 7 October 2005 / Accepted: 27 January 2006 / Published online: 21 March 2006

Abstract Two pumpellyites with the general formula $W_8X_4Y_8Z_{12}O_{56-n}(OH)_n$ were studied using ^{57}Fe Mössbauer spectroscopic and X-ray Rietveld methods to investigate the relationship between the crystal chemical behavior of iron and structural change. The samples are ferrian pumpellyite-(Al) collected from Mitsu and Kouragahana, Shimane Peninsula, Japan. Rietveld refinements gave Fe(X):Fe(Y) ratios (%) of 41.5(4):58.5(4) for the Mitsu pumpellyite and 46(1):54(1) for the Kouragahana pumpellyite, where Fe(X) and Fe(Y) represent Fe content at the X and Y sites, respectively. The Mössbauer spectra consisted of two Fe^{2+} and two Fe^{3+} doublets for the Mitsu pumpellyite, and one Fe^{2+} and two Fe^{3+} doublets for the Kouragahana pumpellyite. In terms of the area ratios of the Mössbauer doublets and the Fe(X):Fe(Y) ratios determined by the Rietveld refinements, $Fe^{2+}(X)$:$Fe^{3+}(X)$:$Fe^{3+}(Y)$ ratios are determined to be 22:14:64 for the Mitsu pumpellyite and 27:8:65 for the Kouragahana pumpellyite. By applying the Fe^{2+}:Fe^{3+}-ratio determined by the Mössbauer analysis and the site occupancies of Fe at the X and Y sites given by the Rietveld method together with chemical analysis, the resulting formula of the Mitsu and Kouragahana pumpellyites are established as $Ca_8(Fe^{2+}_{0.88}Mg_{0.68}Fe^{3+}_{0.77}Al_{1.66})_{\Sigma 3.99}(Al_{5.67}Fe^{3+}_{2.34})_{\Sigma 8.01}Si_{12}O_{42.41}(OH)_{13.59}$ and $Ca_8(Mg_{1.24}Fe^{2+}_{0.65}Fe^{3+}_{0.46}Al_{1.66})_{\Sigma 4.01}(Al_{6.71}Fe^{3+}_{1.29})_{\Sigma 8.00}Si_{12}O_{42.14}(OH)_{13.86}$, respectively. Mean Y–O distances and volumes of the YO_6 octahedra increase with increasing mean ionic radii, i.e., the $Fe^{3+} \rightarrow$ Al substitution at the Y site. However, change of the sizes of XO_6 octahedra against the mean ionic radii at the X site is not distinct, and tends to depend on the volume change of the YO_6 octahedra. Thus, the geometrical change of the YO_6 octahedra with $Fe^{3+} \rightarrow$ Al substitution at the Y site is essential for the structural changes of pumpellyite. The expansion of the YO_6 octahedra by the ionic substitution of Fe^{3+} for Al causes gradual change of the octahedra to more symmetrical and regular forms.

Keywords Pumpellyite · Iron · X-ray Rietveld analysis · Mössbauer spectroscopy

M. Nagashima (✉) · T. Ishida · M. Akasaka
Department of Materials Creation and Circulation Technology, Graduate School of Science and Engineering, Shimane University, 690-8504 Matsue, Japan
E-mail: s039707@matsu.shimane-u.ac.jp
Tel.: +81-852-326455
Fax: +81-852-326469
E-mail: akasaka@riko.shimane-u.ac.jp

Introduction

Pumpellyite is a rock-forming mineral occurring in low-grade metamorphic rocks and hydrothermally altered rocks. Pumpellyite group minerals have monoclinic $A2/m$ symmetry, consist of isolated [SiO_4] tetrahedral and disilicate [$Si_2O_6(OH)$] groups, and contain two symmetrically independent chains of octahedron, oriented parallel to the b-axis. The general formula of pumpellyite is represented as $W_8X_4Y_8Z_{12}O_{56-n}(OH)_n$ (Passaglia and Gottardi 1973). The seven-coordinated W site is primarily occupied by Ca, whereas the tetrahedral Z site is occupied by Si. Both the X and Y sites are octahedral, but the octahedra of the X site are larger than those of the Y site. The X site is occupied by both divalent and trivalent cations including Mg^{2+}, Al^{3+}, Mn^{2+}, Mn^{3+}, Fe^{2+}, Fe^{3+}, and Cr^{3+}, whereas the Y site is occupied only by trivalent cations such as Al^{3+} and Fe^{3+}. Pumpellyite group minerals are named after the most dominant Y site cation (Passaglia and Gottardi 1973); pumpellyite [with Al(Y)] (Palache and Vassar 1925), julgoldite [with $Fe^{3+}(Y)$] (Moore 1971), shuiskite [with $Cr^{3+}(Y)$] (Ivanov et al. 1981), and okhotskite [with $Mn^{3+}(Y)$] (Togari and Akasaka 1987). Recently, a V^{3+}-dominant member of pumpellyite group was approved as a new mineral (IMA No. 2005-018) by the Commission on New Minerals and Mineral Names.

Although iron cations in pumpellyite group minerals commonly exist both as Fe^{2+} and Fe^{3+}, their oxidation state and distribution have not been determined in many

cases due to the difficulty in the determination of Fe oxidation states and site occupancies by conventional chemical analysis. Artioli and Geiger (1994) studied Fe-rich pumpellyites from Keweenawan, Michigan (USA) and Bulla (Italy) using X-ray Rietveld and Mössbauer methods, and concluded that Fe^{2+} and Fe^{3+} were distributed exclusively at the *X* and *Y* sites, respectively. In contrast, Akasaka et al. (1997) analyzed the Mössbauer spectra of Japanese Fe-rich pumpellyites from Tokoro (Hokkaido) and Mitsu (Shimane) and assigned Fe^{2+} to the *X* and *W* sites and Fe^{3+} to the *X* and *Y* sites, based on an assignment scheme differing from that of Artioli and Geiger (1994). Artioli et al. (2003) recently investigated julgoldite-(Fe^{3+}) from Bombay (India) using synchrotron X-ray Rietveld and ^{57}Fe Mössbauer methods, and confirmed the distribution of Fe^{3+} at both the *X* and *Y* sites, which is consistent with the result by Akasaka et al. (1997). However, their Fe^{3+} Mössbauer doublets assignment model differs from those used by Artioli and Geiger (1994) and Akasaka et al. (1997). Moreover, their result raised a several problems for pumpellyite crystal chemistry. Firstly, 95% of the *X* site in the Bombay julgoldite was occupied by trivalent cations. This value deviates considerably from the common ratio (1:1) of divalent and trivalent cations at the *X* site. Secondly, preferential distributions of smaller Al^{3+} and larger Fe^{3+} in the larger *X* and smaller *Y* sites, respectively, contradict the general scheme of cation distribution in common pumpellyite group minerals formulated by Passaglia and Gottardi (1973).

We reinvestigated Fe-rich pumpellyites from Mitsu and Kouragahana, Shimane Peninsula, Japan to solve the problem of differing of ^{57}Fe Mössbauer doublets assignment schemes outlined above, and to examine the crystal chemical behavior of Fe in pumpellyite group minerals. We determined the oxidation states and the site occupancies of Fe using ^{57}Fe Mössbauer and X-ray Rietveld methods, respectively. This paper describes the crystal structures of the Mitsu and Kouragahana Fe-rich pumpellyites and our results for the assignment of ^{57}Fe Mössbauer Fe^{3+} doublets at the *X* and *Y* sites. The relationship between Fe distributions at the *X* and *Y* sites and structural changes is also discussed. In this study, we classified the Mitsu and Kouragahana Fe-rich pumpellyites as pumpellyite-(Al). Hereafter, the pumpellyites from Mitsu and Kouragahana are described as 'MTS' and 'KGH', respectively.

Experimental methods

Sample preparation

The MTS and KGH were collected from hydrothermally altered gabbroic or dolerite sills, cropping out at Shimane Peninsula, Japan. Their occurrences of the Fe-rich pumpellyite and the associated minerals have been described by Kano et al. (1986) and Akasaka et al. (1997, 2003). In the pumpellyite-dominant parts of the samples, needles of pumpellyite crystals form dark green to green cauliflower-like branches up to 0.5 mm in diameter. Crystal aggregates also occur. They are associated with prehnite, calcite, and augite. The pumpellyite aggregates were manually crushed down to grains 0.25–0.5 mm in diameter. Pumpellyite-dominant grains were then separated using a Franz Isodynamic separator. They were further purified by handpicking under a microscope, and treated with dilute HCl solution to remove calcite. The separated grains were crushed further to produce grains 100–150 μm in diameter, and the above purification procedures repeated. Purity of the sample was then confirmed by X-ray powder diffraction analysis.

Chemical analysis

Chemical compositions of the samples were determined using a JEOL JXA-8800M electron probe microanalyzer operated at an accelerating voltage of 15 kV, with beam current of 2.00×10^{-8} A and beam diameter of 1 μm. The standards used were natural wollastonite for Si and Ca, synthetic TiO_2 for Ti, synthetic spinel for Al and Mg, synthetic Cr_2O_3 for Cr, synthetic $Ca_3V_2O_8$ for V, synthetic hematite for Fe, synthetic MnO for Mn, synthetic NiO for Ni and natural anorthoclase for Na and K. Four natural minerals (clinopyroxene, kaersutite, pyrope, and uvarovite) with known compositions were also used as working standards to monitor the precision and accuracy of the analyses. The ZAF method was used for data correction for all elements.

X-ray powder diffraction data collection and Rietveld analysis

Samples were ground manually under alcohol in an agate mortar and pestle until the resultant particle size was less than 5 μm. The powdered sample was then mounted on a glass sample holder with a $20\times15\times0.5$ mm^3 cavity. Mounting for intensity profile collections was made by loading the powder from the front of the holder. Following the method of Raudsepp et al. (1990), a straightedge was used to level the sample surface to that of the holder. The surface was then finely serrated with a razor blade. This technique randomizes the orientation of any anisotropic crystals that are aligned during filling, while maintaining a generally flat surface. The quality of the mounted samples was assessed based on the X-ray rocking curves (ω-scan) for the (115) pumpellyite. These were measured using a RIGAKU RINT automated X-ray powder diffractometer with a normal-focus Cu X-ray tube operated at 35 kV and 25 mA. The instrument was configured with a Bragg–Brentano goniometer equipped with incident- and diffracted-beam soller slits, 0.05° divergence slit, opening of anti-scatter and receiving slits, and a curved graphite diffracted-beam monochromator. Rocking curve profiles at 30.680° 2θ were taken between 10.340

and 20.340° θ, with a step interval of 0.01° and counting time of 5 s/step. The rocking curves obtained were smooth, indicating that the samples were fine-grained and uniform in size.

In collecting step-scan powder diffraction data for the Rietveld analysis, we employed the X-ray powder diffractometer described above equipped with incident- and diffracted-beam soller slits, 1° divergence and anti-scatter slits, and a 0.15 mm receiving slit. The normal-focus Cu X-ray tube was operated at 40 kV and 25 mA. The profiles were taken between 5.00 and 150.00° 2θ with a step interval of 0.02° 2θ. Counting times of MTS and KGH were 7 and 6 s/step, respectively.

The crystal structures of the pumpellyites were refined using the RIETAN-2000 program of Izumi and Ikeda (2000). Single crystal X-ray data for pumpellyite (Yoshiasa and Matsumoto 1985) was used as the initial parameters for the Rietveld refinement in this study. The cell parameters of the pumpellyites determined using a unit-cell parameter refinement program in the RIGAKU RINT system were used as initial values of the Rietveld analysis. The peaks were defined using the "Split Pearson VII function" of Toraya (1990) combined with profile relaxation. An asymmetric parameter is built into this profile function. Details of the profile functions are given by Izumi and Ikeda (2000). Nonlinear least-squares calculation using the Marquardt method was followed by the conjugate-direction method to check convergence at local minima (Izumi 1993). Preferred orientation was corrected using the March-Dollase function (Dollase 1986).

^{57}Fe Mössbauer spectroscopy

The ^{57}Fe Mössbauer spectra of the pumpellyites were measured at room temperature, using 370 MBq ^{57}Co in Pd as a source. The absorbers were about 300 mg of finely ground samples. The Mössbauer data were obtained using a constant acceleration spectrometer fitted with a 1,024 channel analyzer. The isomer shift was referred to a standard metallic iron foil, which was also used to calibrate Doppler velocity. The spectra were fitted to Lorentzians using the least squares method, with line width and intensities constrained to be equal at each site. The QBMOSS program of Akasaka and Shinno (1992) was used for computer analysis. The quality of the fit was judged using the χ^2 value and the standard deviations of the Mössbauer parameters.

Results

Chemical composition

Table 1 gives the average chemical compositions of MTS ($n = 17$) and KGH ($n = 34$), where n represents number of analytical data. Contents of TiO_2, V_2O_3, Cr_2O_3, NiO, and K_2O in MTS and TiO_2, Cr_2O_3, NiO, Na_2O, and K_2O in KGH were less than the EPMA detection limits, and hence were neglected. Numbers of cations were calculated from the analytical data on the basis of 32 total cations. Although Fe is tabulated as total Fe_2O_3 (15.99 wt.%) in MTS to display the standard deviation of Fe content (±0.64 wt.%), the Fe^{2+}:Fe^{3+}-ratio given by the Mössbauer analysis was 0.22:0.78, corresponding to FeO = 3.17 and Fe_2O_3 = 12.47 wt.%. On the other hand, Fe content of KGH is 10.21 ± 0.93 Fe_2O_3 wt.%, and the Fe^{2+}:Fe^{3+}-ratio was 0.27:0.73, corresponding to FeO = 2.48 and Fe_2O_3 = 7.45 wt.%. Following Passaglia and Gottardi (1973), the formulae of MTS and KGH were calculated from the average compositions yielding: $(Ca_{7.98}Na_{0.06})_{\Sigma 8.04}(Fe^{3+}_{2.36}Fe^{2+}_{0.88}Mg_{0.67}Mn^{2+}_{0.05})_{\Sigma 3.96}(Al_{7.25}Fe^{3+}_{0.75})_{\Sigma 8.00}Si_{12.00}O_{42.30}(OH)_{13.70}$ and $(Ca_{7.90}Mn^{2+}_{0.02}Fe^{2+}_{0.08})_{\Sigma 8.00}(Fe^{3+}_{1.75}Fe^{2+}_{0.57}Mg_{1.23}Al_{0.25}V^{3+}_{0.02})_{\Sigma 3.82}Al_{8.00}Si_{12.18}O_{42.38}(OH)_{13.62}$, respectively, where the OH contents were calculated based on the charge balance.

Table 1 Average chemical compositions of the pumpellyite samples (n number of data)

Sample code	MTS		KGH	
Locality	Mitsu, Shimane Peninsula		Kouragahana, Shimane Peninsula	
	$n = 17$		$n = 34$	
	wt. %	s. d.	wt. %	s. d.
SiO_2	36.20	0.36	37.86	0.60
Al_2O_3	18.55	0.51	21.76	0.74
V_2O_3	ND		0.07	0.07
$Fe_2O_3^a$	15.99[b]	0.64	9.93[c]	0.93
MnO	0.17	0.07	0.06	0.03
MgO	1.36	0.19	2.56	0.40
CaO	22.46	0.31	22.91	0.47
Na_2O	0.10	0.04	ND	
	94.83		95.15	
Σ cations = 32				
Si	12.00	0.07	12.18	0.12
Al	7.25	0.16	8.25	0.25
Fe^{3+}	3.99	0.16	2.40	0.24
V^{3+}			0.02	0.02
Mn^{2+}	0.05	0.01	0.02	0.01
Mg	0.67	0.10	1.23	0.11
Ca	7.98	0.07	7.90	0.11
Na	0.06	0.01		

[a]Total Fe as Fe_2O_3
[b]The Fe^{2+}:Fe^{3+}-ratio given by Mössbauer method is 0.22:0.78: Fe^{2+} = 0.88, Fe^{3+} = 3.11 apfu; FeO = 3.17, Fe_2O_3 = 12.47 wt.%
[c]The Fe^{2+}:Fe^{3+}-ratio given by Mössbauer method is 0.27:0.73: Fe^{2+} = 0.65, Fe^{3+} = 1.75 apfu; FeO = 2.41, Fe_2O_3 = 7.25 wt.%

Rietveld analysis

Details of data collection for the Rietveld analyses, the refined unit-cell parameters, R-factors, goodness-of-fit ($S = R_{wp}/R_e$) and the Durbin–Watson d statistic are

Table 2 Data collection and details of structure refinement

Sample code	MTS	KGH
Max. intensity (counts)	6,123	5,567
Space group	*A*2/*m*	
a (Å)	8.8461(2)	8.8335(3)
b (Å)	5.9657(2)	5.9381(3)
c (Å)	19.2016(5)	19.1659(6)
β (°)	97.462(2)	97.446(2)
V (Å^3)	1004.75(5)	996.85(6)
Z	4	4
R_B(%)	3.55	1.92
R_F(%)	1.24	0.82
R_p(%)	6.07	5.78
R_{wp}(%)	7.93	7.62
R_e(%)	5.92	6.26
S	1.340	1.218
D–W *d*	1.174	1.394
Mass fraction		
Pumpellyite	1.000	0.760
Augite		0.125
Prehnite		0.112

Data collection: Step interval (°2*θ*) 5–150°, step 0.02°
Details of structure refinement: Numbers within parentheses represent the standard deviations (1*σ*) and refer to the last digit
R_B *R*-Bragg factor, R_F *R*-structure factor, R_p *R*-pattern, R_{wp} *R*-weighted pattern, R_e *R*-expected, S ($= R_{wp}/R_e$) Goodness of fit (Young 1993), *D–Wd* Durbin–Watson *d*-statistic (Hill and Flack 1987)

Table 3 Site occupancies in *W*, *X*, and *Y* sites

Site	MTS	KGH
*W*1	Ca 1.00	Ca 1.00
*W*2	Ca 1.00	Ca 1.00
X	Mg 0.17	Mg 0.31
	Fe 0.415(4)	Fe 0.278(6)
	Al 0.415(4)	Al 0.415(6)
Y	Fe 0.292(2)	Fe 0.161(3)
	Al 0.709(2)	Al 0.839(3)

The site occupancies of Ca and Mg were fixed by the chemical composition. Estimated standard deviations are in parentheses (1*σ*)

listed in Table 2. The refined powder patterns of MTS and KGH are given in Fig. 1a, b, respectively, indicating that the former is composed solely of pumpellyite and the latter is associated with small amounts of augite and prehnite. Thus, in the Rietveld refinement of KGH, augite and prehnite were added to improve *R*-factors, where structural parameters of augite after Peacor (1967) and prehnite after Akasaka et al. (2003) were used as the initial parameters. Errors are shown by estimated standard deviations of 1*σ* (esd's).

In the structural refinements, Ca was fixed at the *W* site, Mg at the *X* site and Si at the *Z* site based on

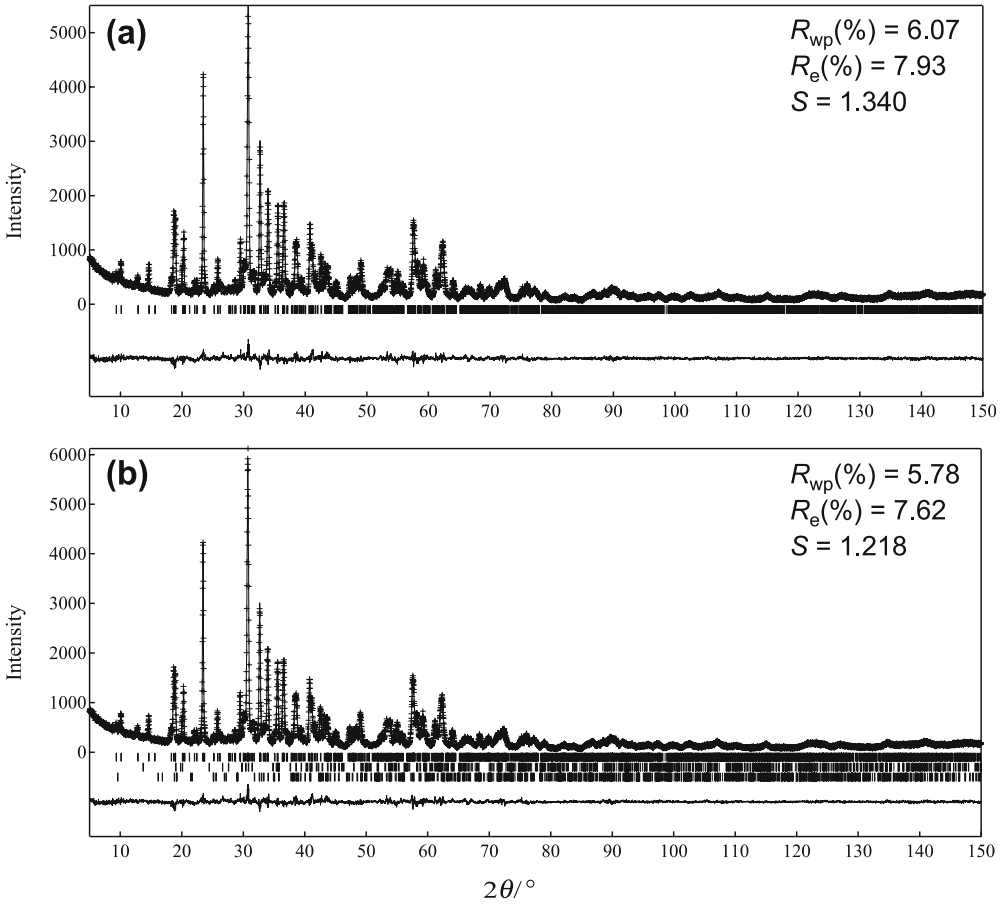

Fig. 1 Rietveld refinement plots for the Mitsu (**a**) and Kouragahana (**b**) pumpellyite-(Al). The Mitsu pumpellyite sample (MTS) was refined with single phase pumpellyite and the Kouragahana pumpellyite sample (KGH) with pumpellyite, augite, and prehnite. The *crosses* are the observed data, the *solid line* is the calculated pattern, and the *vertical bars* mark all possible Bragg reflections (Cu $K\alpha_1$ and $K\alpha_2$). In the plot of KGH (**b**), the *vertical bars* of the top, middle, and bottom correspond to the Bragg reflections of pumpellyite, augite, and prehnite, respectively. The difference between the observed and calculated patterns is shown at the bottom

Table 4 Refined atomic positions

Atom	neq[a]	W^b		MTS	KGH
O1	8	8 *j*	*x*	0.1213(6)	0.1424(8)
			y	0.236(1)	0.230(2)
			z	0.0737(3)	0.0730(4)
			B	0.4(2)	0.8(2)
O2	8	8 *j*	*x*	0.2578(8)	0.261(1)
			y	0.230(1)	0.234(1)
			z	0.2469(3)	0.2473(4)
			B	0.4	0.8
O3	8	8 *j*	*x*	0.3669(6)	0.3628(8)
			y	0.221(1)	0.231(2)
			z	0.4169(3)	0.4153(4)
			B	0.4	0.8
O4	4	4 *i*	*x*	0.1286(9)	0.126(1)
			y	1/2	1/2
			z	0.4425(5)	0.4436(6)
			B	0.4	0.8
O5	4	4 *i*	*x*	0.132(1)	0.137(1)
			y	0	0
			z	0.4592(5)	0.4584(6)
			B	0.4	0.8
O6	4	4 *i*	*x*	0.3664(9)	0.3650(9)
			y	1/2	1/2
			z	0.0463(5)	0.0459(5)
			B	0.4	0.8
O7	4	4 *i*	*x*	0.3730(9)	0.377(1)
			y	0	0
			z	0.0373(5)	0.0365(6)
			B	0.4	0.8
O8	4	4 *i*	*x*	0.0352(9)	0.039(1)
			y	0	0
			z	0.1786(5)	0.1799(3)
			B	0.4	0.8
O9	4	4 *i*	*x*	0.481(1)	0.485(1)
			y	1/2	1/2
			z	0.1743(5)	0.1750(6)
			B	0.4	0.8
O10	4	4 *i*	*x*	0.0712(9)	0.071(1)
			y	0	0
			z	0.3187(5)	0.3168(6)
			B	0.4	0.8
O11	4	4 *i*	*x*	0.5053(8)	0.512(1)
			y	1/2	1/2
			z	0.3155(5)	0.3144(6)
			B	0.4	0.8
*W*1	4	4 *i*	*x*	0.2545(4)	0.2538(4)
			y	1/2	1/2
			z	0.3399(2)	0.3401(2)
			B	0.9(2)	0.5(2)
*W*2	4	4 *i*	*x*	0.1881(3)	0.1870(4)
			y	1/2	1/2
			z	0.1544(2)	0.1557(2)
			B	1.0(2)	1.4(3)
X	4	4 *f*	*x*	1/2	1/2
			y	1/4	1/4
			z	1/4	1/4
			B	0.6(2)	1.4(3)
Y	8	8 *j*	*x*	0.2534(3)	0.2540(4)
			y	0.2510(8)	0.249(1)
			z	0.4946(1)	0.4956(2)
			B	0.6(2)	0.8(2)
Si1	4	4 *i*	*x*	0.0570(5)	0.0531(7)
			y	0	0
			z	0.0922(3)	0.0911(3)
			B	0.8(2)	0.9(3)
Si2	4	4 *i*	*x*	0.1638(5)	0.1644(5)
			y	0	0
			z	0.2496(2)	0.2495(3)
			B	0.4(2)	0.5(2)
Si3	4	4 *i*	*x*	0.4623(6)	0.4645(6)
			y	0	0
			z	0.4017(3)	0.4026(3)
			B	0.9(2)	0.3(2)

Estimated standard deviations are in parentheses (1σ)
[a]Multiplicity
[b]Wyckoff letter

Table 5 Selected interatomic distances (Å) and angles (°)

	MTS	KGH
*W*1–O2 (×2)	2.409(6)	2.384(7)
*W*1–O3 (×2)	2.360(6)	2.278(9)
*W*1–O4	2.386(10)	2.41(1)
*W*1–O8	2.541(8)	2.57(1)
*W*1–O11	2.327(8)	2.40(1)
Mean	2.399(7)	2.386(9)
*W*2–O1 (×2)	2.212(7)	2.25(1)
*W*2–O2 (×2)	2.418(6)	2.387(8)
*W*2–O6	2.766(9)	2.79(1)
*W*2–O9	2.566(9)	2.61(1)
*W*2–O10	2.416(8)	2.40(1)
Mean	2.430(7)	2.44(1)
X–O2 (×2)	2.139(7)	2.109(9)
X–O9 (×2)	2.074(7)	2.058(8)
X–O11 (×2)	1.947(6)	1.925(7)
Mean	2.053(7)	2.031(8)
Y–O1	1.920(6)	1.889(8)
Y–O3	1.913(6)	1.921(7)
Y–O4	2.034(7)	2.048(9)
Y–O5	1.914(6)	1.893(8)
Y–O6	1.992(7)	1.959(7)
Y–O7	1.942(6)	1.947(8)
Mean	1.953(6)	1.943(8)
Si1–O1 (×2)	1.652(7)	1.63(1)
Si1–O4	1.690(9)	1.64(1)
Si1–O8	1.694(9)	1.72(1)
Mean	1.672(8)	1.66(1)
Si2–O2 (×2)	1.607(6)	1.635(8)
Si2–O8	1.659(9)	1.618(9)
Si2–O10	1.648(9)	1.62(1)
Mean	1.630(8)	1.627(9)
Si3–O3 (×2)	1.611(7)	1.68(1)
Si3–O6	1.703(9)	1.69(1)
Si3–O9	1.606(9)	1.61(1)
Mean	1.633(9)	1.67(1)
O1–Si1–O1	116.7(6)	113.0(7)
O1–Si1–O4 (×2)	111.0(3)	112.4(4)
O1–Si1–O8 (×2)	108.8(3)	107.9(4)
O4–Si1–O8	99.1(5)	102.4(6)
O2–Si2–O2	117.0(6)	116.7(7)
O2–Si2–O8 (×2)	106.0(3)	106.3(4)
O2–Si2–O10 (×2)	109.6(4)	107.0(6)
O8–Si2–O10	107.6(4)	110.1(7)
O3–Si3–O3	109.7(6)	110.1(7)
O3–Si3–O6 (×2)	109.(3)	111.6(4)
O3–Si3–O9 (×2)	113.5(3)	110.7(4)
O6–Si3–O9	99.9(5)	101.9(6)

Note: Estimated standard deviations are in parentheses (1σ)

Table 6 The refined and estimated bond lengths of the octahedral sites of samples MTS and KGH

Site	Cation i	V_i	l_0(Å)	l_{ij}(Å)	g_i	Estimated X–O and Y–O lengths (Å)	Observed mean bond lengths (Å)
MTS							
Y	Fe	+3	1.759	2.015	0.292	1.940	1.953(6)
	Al	+3	1.651	1.907	0.709		
Fe(X) = 0.415Fe^{3+}							
X	Mg	+2	1.693	2.099	0.17	1.984	2.053(7)
	Fe	+3	1.759	2.015	0.415		
	Al	+3	1.651	1.907	0.415		
Fe(X) = 0.22Fe^{2+} + 0.19Fe^{3+}							
X	Mg	+2	1.693	2.099	0.17	2.002	2.053(7)
	Fe	+2	1.734	2.140	0.22		
	Fe	+3	1.759	2.015	0.19		
	Al	+3	1.651	1.907	0.415		
KGH							
Y	Fe	+3	1.759	2.015	0.161	1.924	1.943(8)
	Al	+3	1.651	1.907	0.839		
Fe(X) = 0.278Fe^{3+}							
X	Mg	+2	1.693	2.099	0.31	2.002	2.031(8)
	Fe	+3	1.759	2.015	0.278		
	Al	+3	1.651	1.907	0.415		
Fe(X) = 0.16Fe^{2+} + 0.12Fe^{3+}							
X	Mg	+2	1.693	2.099	0.31	2.026	2.031(8)
	Fe	+2	1.734	2.140	0.16		
	Fe	+3	1.759	2.015	0.12		
	Al	+3	1.651	1.907	0.415		

Note: V_i: Oxidation state of cation i. l_0: bond valence parameter (Brown and Altermatt 1985; Brese and O'Keeffe 1991). l_{ij}: expected bond length between cation i and anion j calculated using the equation $V_i = \Sigma \exp[(l_0\text{-}l_{ij})/0.37]$. g_i: refined site occupancy of cation i. Estimated X–O and Y–O lengths: calculated using the equation $x = \Sigma (g_i \times l_{ij})$. Estimated standard deviations are in parentheses (1σ)

published results for single crystal and Rietveld structural refinements of pumpellyite group minerals. Minor amounts of Mn and Na were ignored. Site occupancies of Al and Fe^{3+} in the X and Y sites were refined using the following constraints: $Al(X) = 1.0 - Mg(X) - Fe^{3+}(X)$, $Fe^{3+}(Y) = [\text{total Fe apfu} - 4\times Fe^{3+}(X)]/8$ and $Al(Y) = 1.0 - Fe^{3+}(Y)$ where apfu means atoms per formula unit. The isotropic displacement parameters of oxygen were constrained to be equal. Refined site occupancies are shown in Table 3. The resulting atomic ratios in the X and Y sites of MTS are Mg0.17Fe0.415(4)Al0.415(4) and Fe0.292(4)Al0.709(4), respectively, and those of KGH are Mg0.31Fe0.278(6)Al0.415(6) and Fe0.161(6)Al0.839(6), respectively. The atomic positions are shown in Table 4, and selected interatomic distances and angles are given in Table 5.

The validity of the refined occupancies of Mg, Fe, and Al was examined in terms of the bond lengths estimated from the refined occupancies by using the bond valence sum rule (Brown and Shannon 1973):

$$V_i = \sum_j \exp\left(\frac{l_0 - l_{ij}}{0.37}\right),$$

where V_i is the valence or oxidation state of cation i, l_0 is the bond valence parameter (Brown and Altermatt 1985; Brese and O'Keeffe 1991) and l_{ij} is the bond length between cation i and anion j. Based on this rule, Mg–O, Fe^{2+}–O, Fe^{3+}–O, and Al–O bond lengths at the octahedral sites were calculated to be 2.099, 2.140, 2.015, and 1.907 Å, respectively. Subsequently, X–O and Y–O bond lengths were derived using the equation $x = \sum (g_i \times l_{ij})$, where g_i is the occupancy factor of cation i, and l_{ij} is the bond length between cation i and anion j. On the assumption that all Fe is Fe^{3+}, mean X–O and Y–O bond lengths of MTS were estimated 1.98 and 1.94 Å, respectively (Table 6). The expected mean Y–O distance is similar to the observed one ($\langle Y\text{–O}\rangle = 1.95$ Å). However, the expected mean X–O bond length is considerably shorter than the observed value (2.05 Å). As shown in Table 6, the results for KGH are similar to those of MTS: the expected mean Y–O distance fits to the observed one, but the expected X–O is shorter than the observed value. These results indicate that the refined site occupancies and atomic positions at the Y site are consistent and that Fe is essentially ferric in the Y site, and suggest the presence of Fe^{2+} at the X site.

Mössbauer analysis

The ^{57}Fe Mössbauer spectra of MTS and KGH are shown in Fig. 2 and the hyperfine parameters are listed in Table 7.

The spectrum of MTS consists of four doublets as reported by Akasaka et al. (1997). The doublets AA′ [isomer shift (IS) = 0.38 and quadrupole splitting (QS) = 1.95 mm/s] and BB′ (IS = 0.359 and QS = 1.140 mm/s) are attributed to Fe^{3+}, and those of CC′ (IS = 1.118 and QS = 3.387 mm/s) and DD′

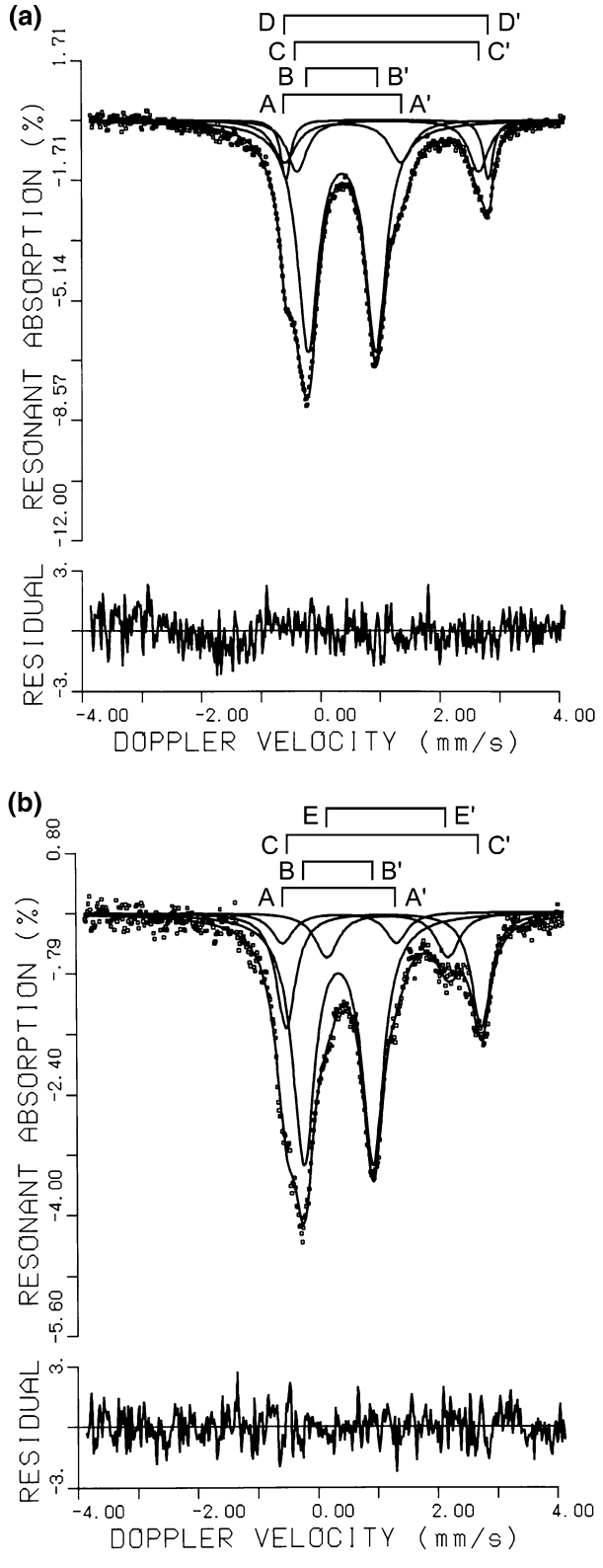

Fig. 2 ^{57}Fe Mössbauer spectra of MTS (**a**) and KGH (**b**) at 298 K. The Mössbauer parameters refined are listed in Table 7

(IS = 1.13 and QS = 3.04 mm/s) to Fe^{2+}. The doublet CC′ is assigned to Fe^{2+} at the *X* site, because a doublet with IS = 1.09–1.14 mm/s and QS = 3.20–3.35 mm/s was assigned to Fe^{2+} at the *X* site by Artioli and Geiger (1994), Akasaka et al. (1997) and Artioli et al. (2003). The doublet DD′ has QS (3.04 mm/s) different from those of Fe^{2+} in pumpellyites reported so far. However, it is rather close to that of Fe^{2+} at the *X* site, and the chemical composition of MTS shows no evidence for the significant substitution of Fe^{2+} for Ca in the *W* site. The DD′ doublet should thus also be assigned to Fe^{2+} at the *X* site. Since QS of $Fe^{2+}(X)$ of the doublet CC′ is larger than that of the doublet DD′, the *X* site characterized by the doublet CC′ is less distorted than that of the doublet DD′, although this slight difference in distortion of the *X* site cannot be detected by the X-ray structure refinement.

The Fe^{3+} doublets with Mössbauer parameters similar to those of the doublets AA′ and BB′ have been assigned to Fe^{3+} at the *Y* sites with different distortions by Artioli and Geiger (1994), Fe^{3+} at the *X* and *Y* sites, respectively, by Akasaka et al. (1997), and Fe^{3+} at the *Y* and *X* sites, respectively, by Artioli et al. (2003). Thus, it is difficult to assign the doublets AA′ and BB′ based on the published assignments. However, assignment of the doublets is possible when the distributions of Fe between the *X* and *Y* sites determined by the X-ray structural refinement are taken into consideration. The amounts

Table 7 ^{57}Fe Mössbauer hyperfine parameters

	MTS	KGH
Doublet	AA′	AA′
IS	0.38(1)	0.384(3)
QS	1.95(2)	1.896(5)
FWHH	0.48(3)	0.437(8)
Area ratio	14(1)	7(1)
Assignment	$Fe^{3+}(X)$	$Fe^{3+}(X)$
Doublet	BB′	BB′
IS	0.359(1)	0.353(8)
QS	1.140(3)	1.154(6)
FWHH	0.422(4)	0.437(8)
Area ratio	64(1)	58(1)
Assignment	$Fe^{3+}(Y)$	$Fe^{3+}(Y)$
Doublet	CC′	
IS	1.118(4)	
QS	3.387(8)	
FWHH	0.20(2)	
Area ratio	8(1)	
Assignment	$Fe^{2+}(X)$	
Doublet	DD′	CC′
IS	1.13(1)	1.115(8)
QS	3.04(3)	3.25(2)
FWHH	0.40(3)	0.386(2)
Area ratio	14(1)	24(1)
Assignment	$Fe^{2+}(X)$	$Fe^{2+}(X)$
Doublet		EE′
IS		1.18(1)
QS		2.02(3)
FWHH		0.468(4)
Area ratio		11(1)
Assignment		$Fe^{2+}(M1)$ in Cpx
χ^2/Freedom	1.27	1.21

Estimated standard deviations are in parentheses (1σ)
IS isomer shift relative to metallic iron absorber (mm/s), *QS* quadrupole splitting (mm/s), *FWHH* full width at half height (mm/s), *Area ratio* %

Table 8 Estimated bond valence (v.u.) in samples MTS and KGH

Anion	Cation								Anion chemistry
	*W*1	*W*2	*X*	*Y*	Si1	Si2	Si3	ΣC^{v}	
MTS									
O1		×2			×2				O^{2-}
		0.46		0.53	0.97			1.96	
O2	×2	×2	×2			×2			O^{2-}
	0.29	0.28	0.29			1.09		1.95	
O3	×2						×2		O^{2-}
	0.32			0.54			1.08	1.94	
O4				×2					O^{2-}
	0.30			0.39	0.87			1.95	
O5				×2					OH^{-}
				0.54				1.08	
O6				×2					O^{2-}
		0.12		0.44			0.84	1.84	
O7				×2					OH^{-}
				0.50				1.00	
O8									O^{2-}
	0.21				0.86	0.95		2.02	
O9			×2×2						O^{2-}
		0.20	0.35				1.10	2.00	
O10									OH^{-}
		0.28				0.98		1.26	
O11			×2×2						OH^{-}
	0.35		0.49					1.33	
ΣA^{v}	2.08	2.08	2.26	2.94	3.67	4.11	4.10		
KGH									
O1		×2			×2				O^{2-}
		0.42		0.55	1.03			2.00	
O2	×2	×2	×2			×2			O^{2-}
	0.30	0.30	0.33			1.01		1.94	
O3	×2						×2		O^{2-}
	0.39			0.51			0.90	1.80	
O4				×2					O^{2-}
	0.29			0.36	1.00			2.01	
O5				×2					OH^{-}
				0.55				1.10	
O6				×2					O^{2-}
		0.11		0.46			0.87	1.90	
O7				×2					OH^{-}
				0.47				0.94	
O8									O^{2-}
	0.19				0.81	1.06		2.06	
O9			×2×2						O^{2-}
		0.18	0.38				1.08	2.02	
O10									OH^{-}
		0.29				1.06		1.35	
O11			×2×2						OH^{-}
	0.29		0.53					1.35	
ΣA^{v}	2.15	2.02	2.48	2.90	3.87	4.14	3.75		

Note: ΣA^{v} is the valence of bonds emanating from cations summed over the bonded anions. ΣC^{v} is the valence of bonds reaching anions. The numbers in the left superscript give the number of identical bonds reaching the anion; the numbers in the right superscripts give the number of identical bonds emanating from cations. Estimated standard deviations are in parentheses (1σ)

of Fe in the *X* and *Y* sites of MTS determined by the Rietveld method are 1.66 and 2.34 apfu, respectively, giving Fe(*X*):Fe(*Y*)-ratio of 41.5:58.5 (%), where Fe(*X*) and Fe(*Y*) represent Fe content at the *X* and *Y* sites, respectively. Area ratios of the Mössbauer doublets AA′, BB′, CC′, and DD′ are 14:64:8:14 (%), which correspond to the amounts of Fe^{3+}, Fe^{3+}, Fe^{2+}, and Fe^{2+}, respectively, and the doublets CC′ and DD′ were attributed to Fe^{2+} at the *X* site, as explained above. Thus, assignment of the doublets AA′ and BB′ to Fe^{3+} at the *X* and *Y* sites (respectively) and the area ratios of the doublets lead to derivation of $Fe^{2+}(X)$:$Fe^{3+}(X)$:$Fe^{3+}(Y)$ ratios of 22:14:64 (%). These values are close to the Fe(*X*):Fe(*Y*)-ratio (=41.5:58.5) determined by the Rietveld method. Consequently, we assign the doublets AA′ and BB′ to Fe^{3+} at the *X* and *Y* site, respectively (Table 7). By applying the Fe^{2+}:Fe^{3+}-ratio determined by the Mössbauer analysis and the site occupancies of Fe at the *X* and *Y* sites given by the Rietveld method, the formula of MTS is established as $Ca_8(Mg_{0.68}Fe^{2+}_{0.88}-Fe_{0.77}{}^{3+}Al_{1.66})_{\Sigma 3.99}(Al_{5.67}Fe_{2.34}{}^{3+})_{\Sigma 8.01}Si_{12}O_{42.41}(OH)_{13.59}$, where the OH content is calculated based on the charge balance.

The spectrum of KGH is composed of three doublets of pumpellyite and one doublet of Ca-clinopyroxene. The doublets AA′ (IS = 0.384 and QS = 1.896 mm/s) and

BB′ (IS = 0.353 and QS = 1.154 mm/s) are attributed to Fe^{3+}, and those of CC′ (IS = 1.115 and QS = 3.25 mm/s) to Fe^{2+} of pumpellyite. The doublet EE′ with IS = 1.18 and QS = 2.02 mm/s is assigned to Fe^{2+} at *M1* site of Ca-clinopyroxene (Matsui et al. 1970; Bancroft et al. 1971; Akasaka 1990). Since the average chemical composition ($n = 5$) of augite as an impurity in the KGH sample is 50.54 SiO_2, 0.38 TiO_2, 3.49 Al_2O_3, 0.10 V_2O_3, 0.34 total MnO, 12.65 total FeO, 13.83 MgO, 19.10 CaO, 0.41 Na_2O, 0.04 K_2O and 100.84 wt.% total, all Fe is considered as ferrous iron. The amounts of Fe in the *X* and *Y* sites of KGH, determined by the Rietveld method, are 1.11 and 1.29 apfu, respectively, which is recalculated to Fe(*X*):Fe(*Y*)-ratio of 46.3:53.7 (%). Area ratios of the Mössbauer doublets AA′, BB′, and CC′ are 8:65:27 (%), which correspond to the amounts of Fe^{3+}, Fe^{3+}, and Fe^{2+} in KGH, respectively. Thus, the Fe^{2+} (*X*):Fe^{3+} (*X*):Fe^{3+} (*Y*) ratio of 27:8:65 (%) derived from the assignments of the doublets AA′, BB′, and CC′ to Fe^{3+}(*X*), Fe^{3+}(*Y*), and Fe^{2+}(*X*), respectively, is most close to the Fe distributions (Fe(*X*):Fe(*Y*) = 46.3:53.7%) determined by the Rietveld method. By using the same calculation scheme of the formula as MTS, the formula of KGH is established as $Ca_8(Mg_{1.24}Fe^{2+}_{0.65}Fe^{3+}_{0.46}Al_{1.66})_{\Sigma 4.01}(Al_{6.71}Fe^{3+}_{1.29})_{\Sigma 8.00}Si_{12}O_{42.14}(OH)_{13.86}$.

These results indicate that, in MTS and KGH, Al^{3+} cations are dominant both in the *Y* and *X* sites, and, thus, these pumpellyites are classified as 'pumpellyite-(Al)' in spite of the high Fe^{3+} contents.

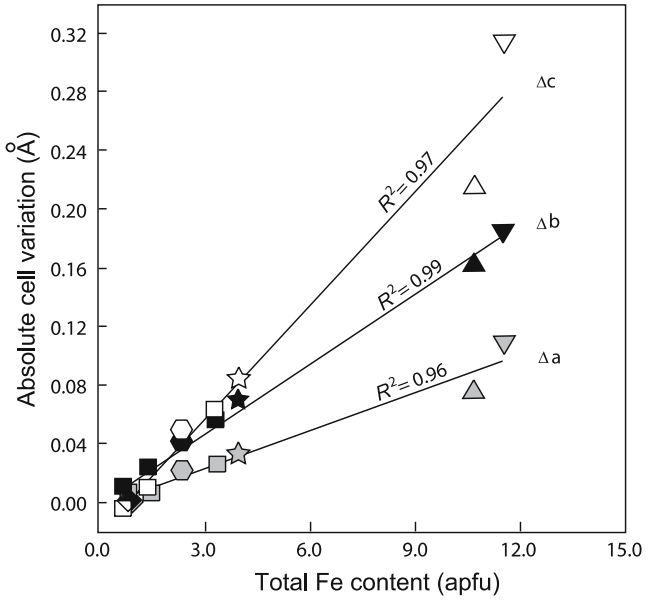

Fig. 3 Variation of the unit-cell parameters as a function of the total Fe content (atoms per formula unit: apfu) in pumpellyites and julgoldites. *Gray symbols* refer to the *a*-axis, closed symbols to the *b*-axis, and open symbols to the *c*-axis. Symbols and sources: *inverted triangles* (Allmann and Donnay 1973), *diamonds* (Yoshiasa and Matsumoto 1985), *squares* (Artioli and Geiger 1994), *triangles* (Artioli et al. 2003), *stars* (MTS of this study), and *hexagon* (KGH of this study)

Discussion

Atomic configurations at the *X* and *Y* sites and local charge neutralization

As noted above, the expected *Y*–O bond distances of MTS and KGH derived from the refined occupancies of Fe and Al at the *Y* site using bond valence sum rule are consistent with the observed *Y*–O distances, indicating that the atomic configuration in the *Y* site is in harmony with the refined atomic positions and that Fe is essentially ferric in the *Y* site. However, in the case that all Fe

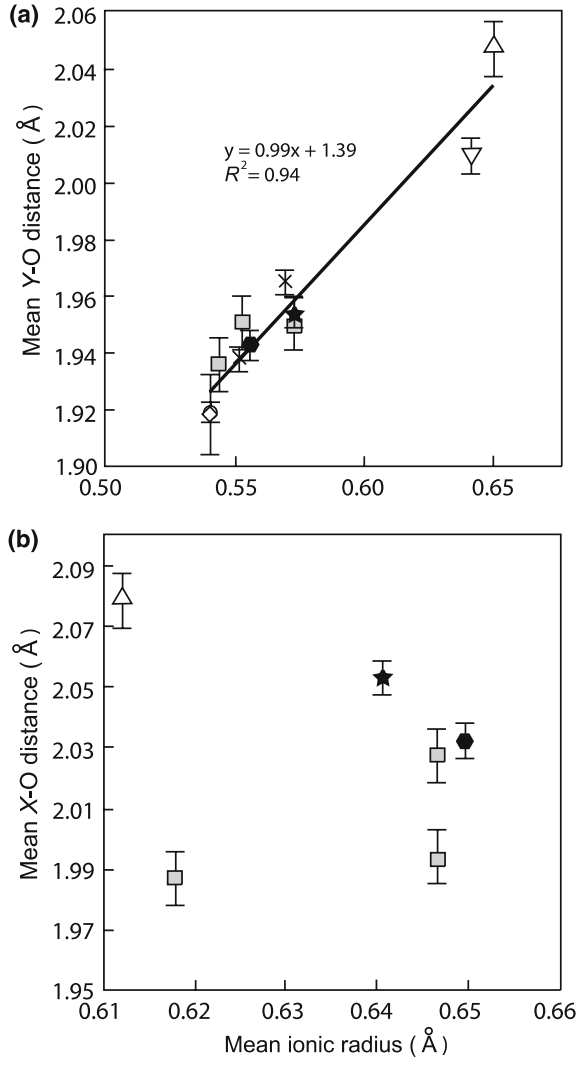

Fig. 4 **a** The relationship between mean ionic radii at the *Y* site and mean *Y*–O distances. **b** The relationship between mean ionic radii at the *X* site and mean *X*–O distances. Mean ionic radii were calculated by using the ionic radii of Shannon (1976). Symbols and sources: *open circle* (Galli and Alberti 1969), *open inverted triangle* (Allmann and Donnay 1973), *open diamond* (Yoshiasa and Matsumoto 1985), *gray squares* (Artioli and Geiger 1994), *crosses* (Artioli et al. 1996), *open triangle* (Artioli et al. 2003), *filled star* (MTS of this study), and *filled hexagon* (KGH of this study)

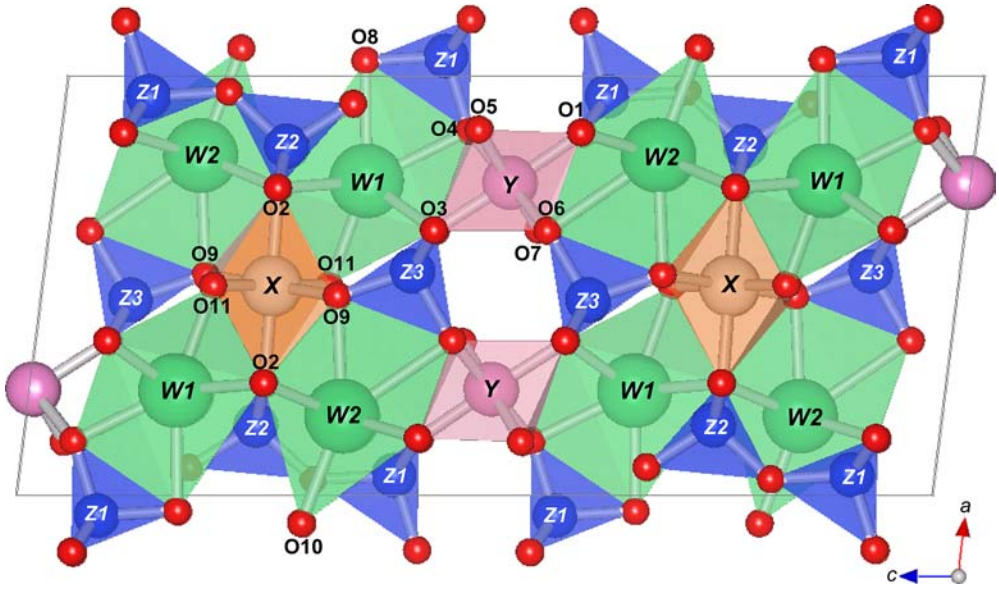

Fig. 5 Crystal structure of MTS on *a*–*c* plane drawn with VICS developed by Dilanian and Izumi (Izumi 2005)

is assumed as Fe^{3+}, the expected *X*–O distances were shorter than the observed values, suggesting the presence of Fe^{2+} in the *X* site. Thus, *X*–O distances were re-estimated using the resulting atomic ratios of $Mg:Fe^{2+}:Fe^{3+}:Al = 0.17:0.22:0.19:0.415$ for MTS and 0.31:0.16:0.12:0.415 for KGH. As shown in Table 6, the *X*–O distance of MTS is calculated to be 2.00 Å, close to the observed value of 2.05 Å, and that of KGH is calculated to be 2.03 Å, same as the observed value of 2.03 Å. Thus, the resulting $Fe^{2+}:Fe^{3+}$-ratio and the atomic configuration are consistent with the results of structural refinements.

The local neutralization of charge in the structures of MTS and KGH was also examined in terms of the bond valence sum calculated after the method of Donnay and Allmann (1970) (Table 8). The bond valence sums of the *W*1, *W*2, *Y*, and *Z* sites of MTS and KGH are close to the expected values, and the sum of the *X* site is 2.26 and 2.48, respectively, indicating the presence of both divalent and trivalent cations in this site. The sums of O5 and O7 are sufficiently close to the expected value of 1 for an hydroxyl group, whereas those for O10 and O11 are 1.26 and 1.33 for MTS and 1.35 and 1.35 for KGH, respectively. These values are consistent with those for pumpellyite obtained by Yoshiasa and Matsumoto (1985). They suggested that the substitution $M^{2+}(X) + H^{+}(H11) + O^{2-}(O11) \leftrightarrow M^{3+}(X) + O^{2-}(O11)$, which reduces the number of hydrogen atoms, possibly occurs at the *X* site.

Relationship between unit cell parameters and mean bond lengths at the *X* and *Y* sites

Published studies of the pumpellyite–julgoldite series indicate that the unit-cell parameters *a*, *b*, *c*, and cell volume increase with increasing Fe content, and that $Al \leftrightarrow Fe^{3+}$ substitution at the *Y* site has a significant effect on unit-cell parameters (Passaglia and Gottardi 1973; Artioli and Geiger 1994; Akasaka et al. 1997; Artioli et al. 2003). Cell parameters of MTS and KGH plot on the regression lines in the absolute cell variation—total Fe content diagram (Fig. 3), consistent with the positive relationships between cell parameters and total Fe contents.

The changes in bond lengths at the *X* and *Y* sites have not been clarified in terms of the ionic substitutions at these sites, however. The mean *Y*–O distance correlate well with the mean ionic radius, calculated based on the ionic radii by Shannon (1976), as shown in Fig. 4a, which causes expansion of the *Y* site and increase of the unit-cell parameters. The edges of the YO_6 octahedra may dominate the variation of each cell dimension as follows; O1–O6, O3–O4, O3–O5, O4–O7, and O5–O6 edges for *a*-axis, O4–O5, O6–O7, O1–O4, O1–O5, O3–O6, and O3–O7 edges for *b*-axis, and O1–O5, O3–O7, O1–O4, O3–O6, O5–O6 and O4–O7 edges for *c*-axis. Since the edges of O1–O4, O1–O5, O3–O6 and O3–O7 are not shared with other polyhedra (Fig. 5), they elongate more straightforward than the other shared edges with the $Fe^{3+} \rightarrow Al$ substitution at the *Y* site, which easily causes the increase in the *c*-dimension than the *a*- and *b*-dimensions.

The relationship between the ionic substitutions and the structural changes at the *X* site is not simple, because both divalent and trivalent cations occur in this site and M^{2+}/M^{3+}-ratios differ from sample to sample. For example, mean ionic radii at the *X* site of MTS, KGH, and Bombay julgoldite-(Fe^{3+}) are calculated 0.641, 0.650, and 0.612 Å, respectively. However, in contrast to the expectation in terms of the mean ionic radii, mean *X*–O distances of 2.05 ± 0.01 Å (volume: 11.5 $Å^3$) for

MTS and 2.031 ± 0.008 Å (volume: 11.1 Å^3) for KGH are almost the same as the value of 2.08 ± 0.01 Å (volume: 11.9 Å^3) for Bombay julgoldite-(Fe^{3+}), and, thus, there is no correlation between the mean ionic radii and the mean *X*–O distances (Fig. 4b). The insignificance of ionic substitutions at the *X* site to the size of the XO_6

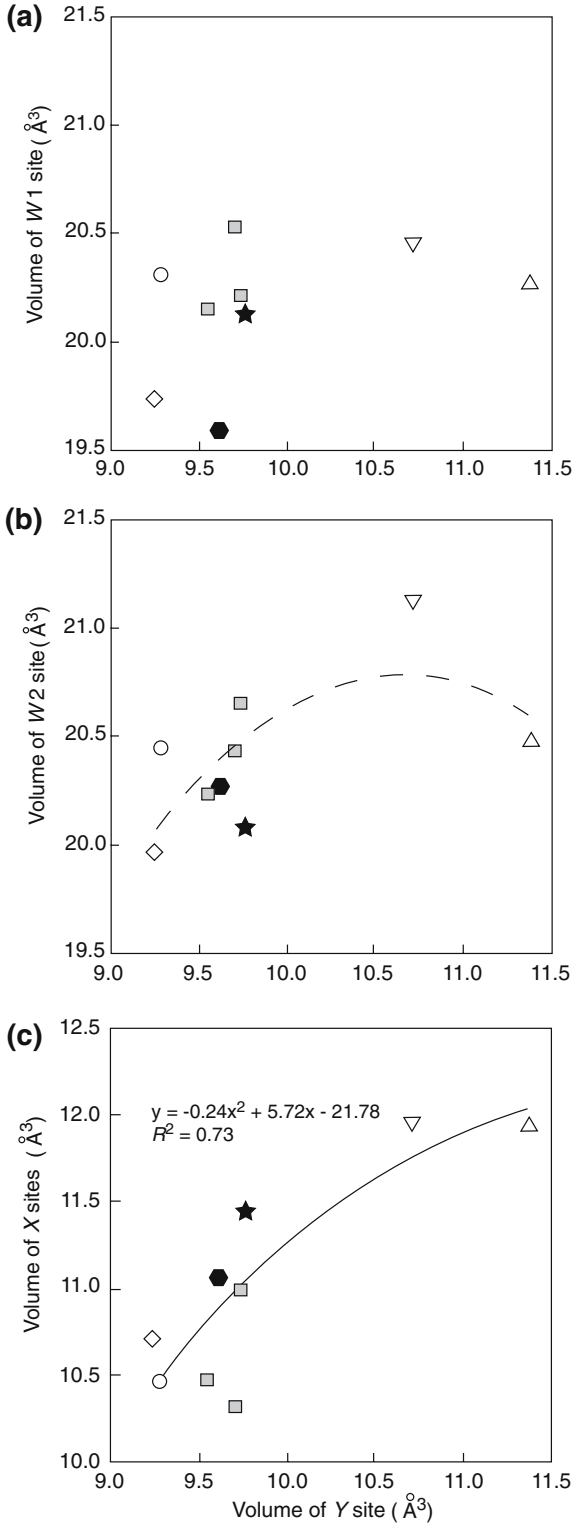

Fig. 6 Relationships of volumes of **a** the $W1O_7$ polyhedra, **b** the $W2O_7$ polyhedra, and **c** the XO_6 octahedra versus that of the YO_6 octahedra. Symbols and sources as in Fig. 4

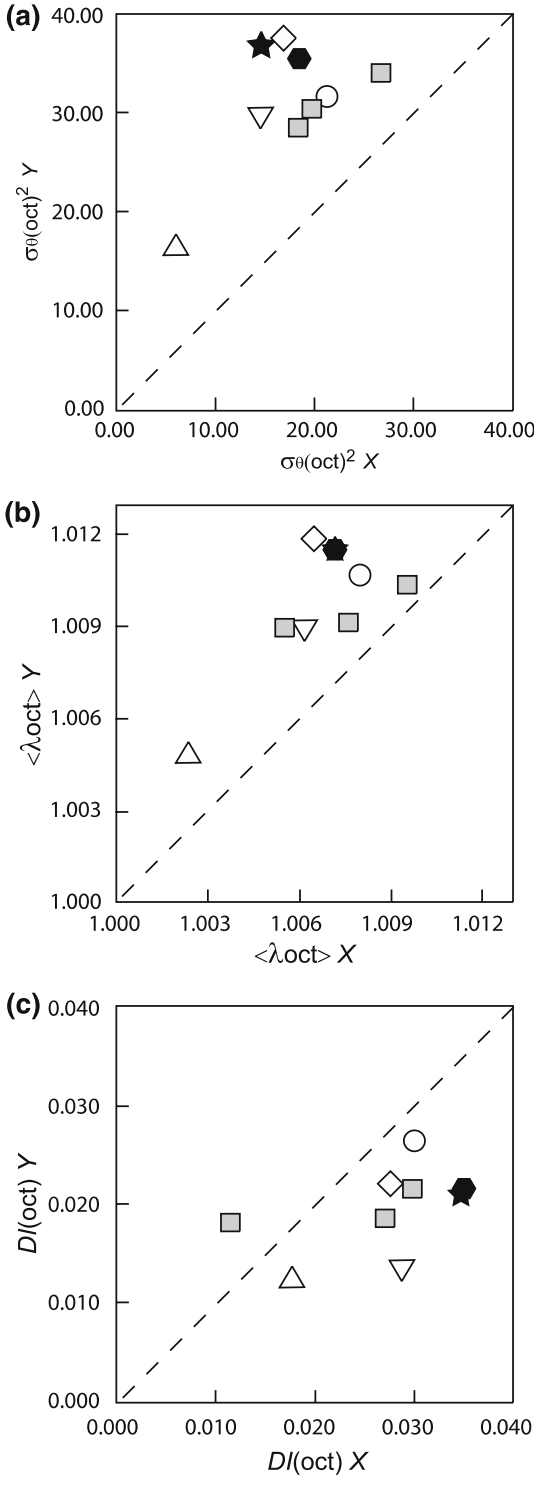

Fig. 7 Relationship of site distortions between the *X* and *Y* sites. **a** $\sigma_\theta(\mathrm{oct})^2_X$–$\sigma_\theta(\mathrm{oct})^2_Y$, **b** $\langle\lambda_{\mathrm{oct}}\rangle_X$–$\langle\lambda_{\mathrm{oct}}\rangle_Y$, and **c** $\mathrm{DI(oct)}_X$–$\mathrm{DI(oct)}_Y$. Definitions of the distortion parameters are shown in Table 9. Symbols and sources as in Fig. 4

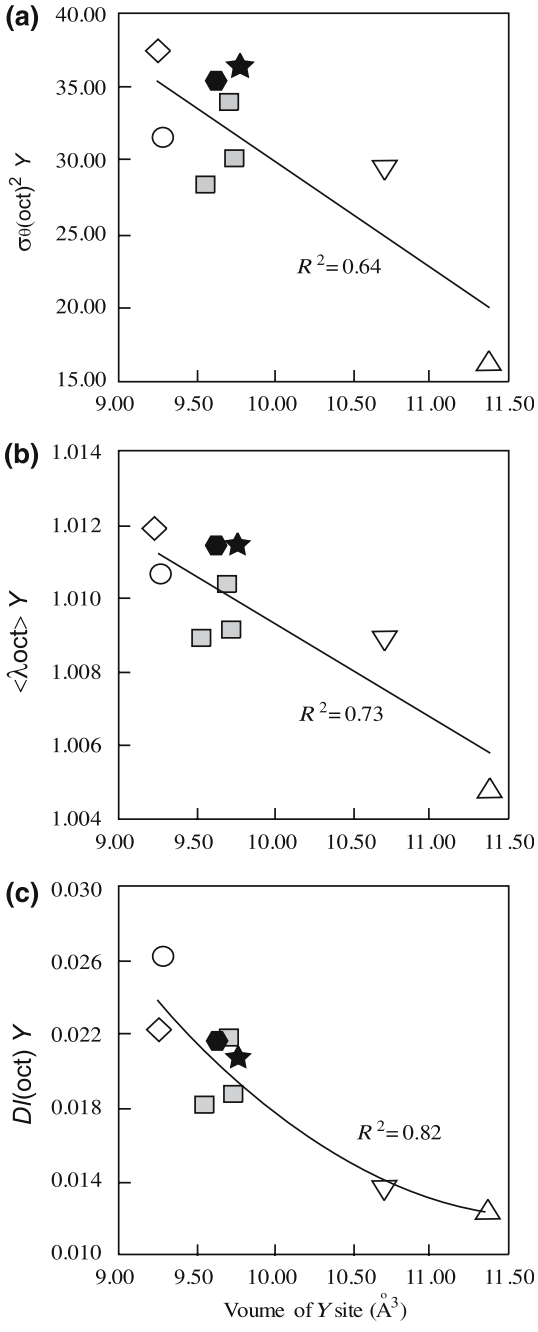

Fig. 8 Relationship between the volumes and distortions of the YO_6 octahedra. **a** V_Y–$\sigma_\theta(\mathrm{oct})^2_Y$ (Robinson et al. 1971), **b** V_Y–$\langle\lambda_{\mathrm{oct}}\rangle_Y$ (Robinson et al. 1971), and **c** V_Y–$\mathrm{DI(oct)}_Y$ (Baur 1974). Definitions of the distortion parameters are given in Table 9. Symbols and sources as in Fig. 4

octahedra may be interpreted in terms of the following facts: (1) the size of XO_6 octahedra is essentially large; (2) all edges of octahedra of the X site are shared with the $W1$ and $W2$ polyhedra (Fig. 5), which prohibits changes of the size of the XO_6 octahedra.

Due to the sharing of the O1–O6 edge between the Y and $W2$ sites and of the O3–O5 edge between the Y and $W1$ sites, the volumes of the $W2O_7$ and $W2O_7$ polyhedra increase with increasing the volume of the YO_6 octahedra by the $Fe^{3+} \rightarrow Al$ substitution at the Y site (Fig. 6a, b). The enlargements of $W1O_7$ and $W2O_7$ polyhedra elongate the edges shared with X site. Finally, the volume of the X site is influenced by that of the Y site (Fig. 6c).

Site distortion of the X and Y sites

In contrast to the previous Mössbauer studies of Fe-rich pumpellyite by Akasaka et al. (1997), the doublets AA′ with QS = 1.896–1.95 mm/s and BB′ with QS = 1.14–1.154 mm/s in our Mössbauer spectra are assigned to Fe^{3+} at the X and Y sites, respectively. This result supports the Fe^{3+} doublets assignments of Artioli et al. (2003) that the doublets with QS about 1.7 mm/s and about 1.1 mm/s to $Fe^{3+}(X)$ and $Fe^{3+}(Y)$, respectively. However, these assignments seem to contradict the well known theoretical and empirical rule that the QS of Fe^{3+} at the distorted site is greater than that at the less distorted site (Bancroft et al. 1967). Using the polyhedral distortion indices of Robinson et al. (1971), Artioli and Geiger (1994) and Akasaka et al. (1997) indicated that site distortion of the Y site is greater than that of the X site. This requires larger QS for Fe^{3+} at the Y site than that at the X site. Thus, the distortions of the X and Y sites in pumpellyites were re-examined in terms of the bond length distortion parameters $\langle\lambda_{\mathrm{oct}}\rangle$ defined by Robinson et al. (1971), DI(oct) by Baur (1974), and the angular distortion parameter $\sigma_\theta(\mathrm{oct})^2$ by Robinson et al. (1971).

The angular distortion and bond length distortion parameters of MTS and KGH are listed in Table 9, along with those of pumpellyites and julgoldites from other localities. As pointed out by Artioli and Geiger (1994), the $\sigma_\theta(\mathrm{oct})_X^2$–$\sigma_\theta(\mathrm{oct})_Y^2$ and $\langle\lambda_{\mathrm{oct}}\rangle_X$–$\langle\lambda_{\mathrm{oct}}\rangle_Y$ diagrams (Fig. 7a, b) reveal larger angular and bond length distortions of the Y site than those of the X site. However, in terms of the DI(oct) of Baur (1974), bond length distortions of the X site [excepting one sample from Artioli and Geiger (1994)] are larger than those at the Y site (Fig. 7c). In the case of their study of synthetic piemontite having three kinds of octahedral sites, Nagashima and Akasaka (2004) found that the DI(oct) parameter is more sensitive to bond length distortions than that of Robinson et al. (1974). The DI(oct) parameter may also be a more practical indicator of the bond length distortions of octahedra in pumpellyite.

All site distortion parameters, such as $\sigma_\theta(\mathrm{oct})^2$, $\langle\lambda_{\mathrm{oct}}\rangle$, and DI(oct), for the Y site tend to decrease with increasing mean Y–O distance and volume of the Y site (Fig. 8). This observation confirms that expansion of the YO_6 octahedra caused by ionic substitutions results in gradual change to highly symmetrical and regular form.

Table 9 Angular and bond length distortions of the *X* and *Y* octahedral sites

Sample	*X* site			*Y* site			Reference
	$\sigma_\theta(\text{oct})^2$	$\langle\lambda_{\text{oct}}\rangle$	DI	$\sigma_\theta(\text{oct})^2$	$\langle\lambda_{\text{oct}}\rangle$	DI	
MTS	14.41	1.007	0.034	36.39	1.012	0.021	This study
KGH	18.41	1.008	0.035	35.25	1.011	0.022	This study
HR	21.08	1.008	0.030	31.63	1.011	0.026	Galli and Alberti (1969)
Julgoldite	14.55	1.006	0.029	29.59	1.009	0.014	Allmann and Donnay (1973)
Pumpellyite	16.83	1.007	0.028	37.46	1.012	0.022	Yoshiasa and Matsumoto (1985)
HR	18.20	1.006	0.011	28.39	1.009	0.018	Artioli and Geiger(1994)
K1	26.64	1.010	0.030	34.01	1.010	0.022	
BU	19.79	1.008	0.027	30.16	1.009	0.019	
Bombay julgoldite-(Fe^{3+})	5.98	1.002	0.018	16.30	1.005	0.012	Artioli et al. (2003)

Note: HR, K1, and BU are sample codes defined by Galli and Alberti (1969), and Artioli and Geiger (1994). $\langle\lambda_{\text{oct}}\rangle = \sum_{i=1}^{6}(l_i - l_0)^2/6$ (l_i: each bond length, l_0: center-to-vertex distance for an octahedron with O_h symmetry whose volume is equal to that of strained or distorted octahedron with bond lengths l_i) (Robinson et al. 1971), DI(oct) $= 1/6\Sigma\,|R_i - R_{\text{av.}}|/R_{\text{av.}}$ (R_i: each bond length, $R_{\text{av.}}$: average distance for an octahedron) (Baur 1974), and $\sigma_\theta(\text{ oct})^2 = \sum_{i=1}^{12}(\theta_i - 90^\circ)^2/11$ (θ_i: O–*M*–O angle) (Robinson et al. 1971)

Acknowledgements Our thanks to Dr. Fujio Izumi of the National Institute for his permission to use the RIETAN-2000 and VICS programs and for his helpful advice; to Dr. Kuniaki Makino of Shinshu University for helpful discussion on crystal structure analysis; and to Dr. Barry Roser of Shimane University for comment on the manuscript; Mr. Chihiro Fukuda for providing the Kouragahana pumpellyite-(Al) sample. A part of this work was supported by the Sasakawa Scientific Research Grant from the Japan Science Society to Mariko Nagashima (No. 17-105).

References

Akasaka M (1990) Clinopyroxene on the join $CaMgSi_2O_6$–$CaFe^{3+}AlSiO_6$–$CaTiAl_2O_6$ at low oxygen fugacity. Proc Indian Acad Sci (Earth Planet Sci) 99:39–48

Akasaka M, Shinno I (1992) Mössbauer spectroscopy and its recent application to silicate mineralogy (in Japanese). J Mineral Soc Japan 21:3–20

Akasaka M, Kumura Y, Omori Y, Sakakibara M, Shinno I, Togari K (1997) ^{57}Fe Mössbauer study of pumpellyite–okhotskite–julgoldite series minerals. Mineral Petrol 61:181–198

Akasaka M, Hashimoto H, Makino K, Hino R (2003) ^{57}Fe Mössbauer and X-ray Rietveld studies of ferrian prehnite from Kouragahana, Shimane Peninsula, Japan. J Mineral Petrol Sci 98:31–40

Allmann R, Donnay G (1973) The crystal structure of julgoldite. Miner Mag 39:271–281

Artioli G, Geiger CA (1994) The crystal chemistry of pumpellyite: an X-ray Rietveld refinement and ^{57}Fe Mössbauer study. Phys Chem Minerals 20:443–453

Artioli G, Pavese A, Belotto M, Collins SP, Luchetti G (1996) Mn crystal chemistry in pumpellyite: a resonant-scattering powder diffraction Rietveld study using synchrotron radiation. Am Mineral 81:603–610

Artioli G, Geiger CA, Dapiaggi M (2003) The crystal chemistry of julgoldite-Fe^{3+} from Bombay, India, studied using synchrotron X-ray powder diffraction and ^{57}Fe Mössbauer spectroscopy. Am Mineral 88:1084–1090

Bancroft GM, Maddock AG, Burns RG (1967) Applications of the Mössbauer effect to silicate mineralogy—I. Iron silicates of known crystal structure. Geochim Cosmochim Acta 31:2219–2246

Bancroft GM, Williams PGL, Burns RG (1971) Mössbauer spectra of minerals along the diopside-hedenbergite tie line. Am Mineral 56:1617–1625

Baur H (1974) The geometry of polyhedral distortions. Predictive relationships for the phosphate group. Acta Crystallogr B 30:1195–1215

Brese NE, O'Keeffe M (1991) Bond-valence parameters for solids. Acta Crystallogr B 47:192–197

Brown ID, Altermatt D (1985) Bond-valence parameters obtained from a systematic analysis of the inorganic crystal structure database. Acta crystallogr B 41:244–247

Brown ID, Shannon RD (1973) Empirical bond-strength–bond-length curves for oxides. Acta Crystallogr A 29:266–282

Dollase WA (1986) Correction of intensities for preferred orientation in powder diffractometry: application of the March model. J Appl Crystallogr 19:267–272

Donnay G, Allmann R (1970) How to recognize O^{2-}, OH-, and H_2O in crystal structures determined by X-rays. Am Mineral 55:1003–1015

Galli E, Alberti A (1969) On the crystal structure of pumpellyite. Acta Crystallogr B 25:2276–2281

Hill RJ, Flack HD (1987) The use of the Durbin–Watson *d* statistic in Rietveld analysis. J Appl Crystallogr 20:356–361

Ivanov OK, Arkhangel'skaya VA, Miroshnikova LO, Shilova TA (1981) Shuiskite, the chromium analogue of pumpellyite, from the Bisersk deposit, Urals (in Russian). Zapiski Vsesoyuznogo Mineralogicheskogo Obshchestva 110:508–512

Izumi F (1993) Rietveld analysis program RIETAN and PREMOS and special applications. In: Young RA (ed) The Rietveld method. Oxford Science Publications, Oxford, pp 236–253

Izumi F (2005) VENUS system for three-dimensional visualization of crystal structures and electronic states (in Japanese with English abstract). Rigaku J 36:18–27

Izumi F, Ikeda T (2000) A Rietveld analysis program RIETAN-98 and its application to zeolites. Material Science Forum 321–324

Kano K, Satoh H, Bunno M (1986) Iron-rich pumpellyite and prehnite from the Miocene gabbroic sills of the Shimane Peninsula, Southwest Japan. J Jpn Assoc Mineral Petrol Econ Geol 81:51–58

Matsui Y, Maeda Y, Shono Y (1970) Mössbauer study of synthetic calcium-rich pyroxenes. Geochem J 14:15–26

Moore PB (1971) Julgoldite, the Fe^{2+}–Fe^{3+} dominant pumpellyite. A new mineral from Långban, Sweden. Lithos 4:93–99

Nagashima M, Akasaka M (2004) An X-ray Rietveld study of piemontite on the join $Ca_2Al_3Si_3O_{12}(OH)$–$Ca_2Mn^{3+}{}_3Si_3O_{12}(OH)$ formed by hydrothermal synthesis. Am Mineral 89:1119–1129

Palache C, Vassar HE (1925) Some minerals of the Keweenawan copper deposits: a new mineral; sericite, saponite. Am Mineral 10:412–428

Passaglia E, Gottardi G (1973) Crystal chemistry and nomenclature of pumpellyites and julgoldites. Can Mineral 12:219–223

Peacor DR (1967) Refinement of the crystal structure of a pyroxene of formula $M_IM_{II}(Si_{1.5}Al_{0.5})O_6$. Am Mineral 52:31–41

Raudsepp M, Hawthorne FC, Turnock AC (1990) Evaluation of the Rietveld method for the characterization of fine-grained products of mineral synthesis: the diopside–hedenbergite join. Can Mineral 28:93–109

Robinson K, Gibbs GV, Ribbe PH (1971) Quadratic elongation: a quantitative measure of distortion in coordination polyhedra. Science 172:567–570

Shannon RD (1976) Revised effective ionic radii and systematic studies of interatomic distances in halides and chalcogenides. Acta Crystallogr A 32:751–767

Togari K, Akasaka M (1987) Okhotskite, a new mineral, an Mn^{3+}-dominant member of the pumpellyite group, from the Kokuriki mine, Hakkaido, Japan. Min Mag 51:611–614

Toraya H (1990) Array-type universal profile function for powder pattern fitting. J Appl Crystallogr 23:485–491

Yoshiasa A, Matsumoto T (1985) Crystal structure refinement and crystal chemistry of pumpellyite. Am Mineral 70:1011–1019

Young RA (1993) Introduction to the Rietveld method. In: Young RA (ed) The Rietveld method. Oxford Science Publications, Oxford, pp 1–38